第36卷第1期
2017年2月

红外与毫米波学报
J. Infrared Millim. Waves

Vol. 36, No. 1
February, 2017

文章编号: 1001 - 9014(2017)01 - 0035 - 07

DOI:10.11972/j.issn.1001 - 9014.2017.01.008

A W-band digital variable polarimetric radar for target characteristic measurement

LI Zhang-Feng, HU Bing*, ZHAO Guo-Qiang, LI Shi-Yong, SUN Hou-Jun, TAO Ran

(School of Information and Electronic, Beijing Institute of Technology, 100081, China)

Abstract: A novel W-band digital variable polarimetric radar for target characteristic measurement is presented in this paper. The main components of the digital variable polarimetric radar are the two-subarrays variable polarized antenna, the two-channels T/R modules, and the digital signal processing unit. This radar transmits arbitrary polarized electromagnetic wave by spatial polarimetric synthesis, and receives arbitrary polarized echo by digital polarimetric synthesis. The experimental results illustrate that the W-band digital variable polarized measurement radar can extract the polarimetric scattering matrix accurately under various polarimetric modes, has the ability of measuring full-pol RCS of the target and can be used for target polarimetric information analyzing and research.

Key words: millimeter-wave radar, polarimetric scattering characteristics, polarimetric measurement radar
PACS: 84.40.Xb

W 波段数字变极化目标特性测量雷达

李璋峰, 胡 冰*, 赵国强, 李世勇, 孙厚军, 陶 然
(北京理工大学信息与电子学院,北京 100081)

摘要:提出一种新型的W波段数字变极化目标特性测量雷达.该雷达由两子阵变极化天馈、两通道TR模块与数字处理单元构成,采用空间波束合成任意极化发射、数字方式实现任意极化接收.通过目标实验结果表明,该雷达能在多种极化体制下准确提取目标极化散射矩阵,具备测量目标全极化RCS能力以及可用于目标极化特性分析与研究.

关 键 词:毫米波雷达;极化散射特性;极化测量雷达

中图分类号:TN959.6 **文献标识码**:A

Introduction

Target informations such as the range, speed and high-resolution are acquired by radar through analyzing the time delay, frequency and phase of the echo. The same as time, frequency, and phase, polarization is also an important representation of the electromagnetic wave. The traditional single polarized radar cannot measure the polarization characteristics of the target echo, such that it will miss the polarimetry information of the target. The polarimetric scattering characteristics, as a description of the size, structure, and material of the target, plays an important role in the target recognition, classification, and identification. They are widely applied in remote sensing[1], meteorological detection[2], and low RCS target detection[3], etc. For target polarimetric scattering characteristics analyze and research, the polarimetric radar is a necessary tool which needs to be carefully considered and designed.

The polarimetric mode is a basic issue for the polarimetric radar, which has an important influence on the complexity, waveform design, signal processing, and system performance. The MEMPHIS is a multi-frequency experimental monopulse high-resolution interferometric SAR, which achieves the dual-pol and the full-pol modes under linear polarized base by the dual-pol parabolic antenna and the angulation by the monopulse comparator[4-5]. The L-band Microwave Imaging Radiometer with Aperture Synthesis (MIRAS) of the European Space A-

Received date: 2016-06-08, **revised date**: 2016-07-21 **收稿日期**:2016-06-08, **修回日期**:2016-07-21
Foundation items: Supported by National Natural Science Foundation of China (61301191)
Biography: Li Zhang-Feng(1989-), male, Zhuzhou County, Hunan, Ph. D. Research area involves polarimetric millimeter-wave radar, polarimtric information processing and micro-Doppler effect. E-mail: lizhangfeng@bit.edu.cn
* **Corresponding author**: E-mail: hubing@bit.edu.cn

gency can work in the dual-pol and the full-pol modes based on a dual-pol antenna and the polarization switches under linearly polarized base[6]. The X-band phased array weather radar of the Raytheon Company also introduces the dual-pol technique [7]. The compact polarimetric mode has drawn more and more attentions in recent years[8]. The Japanese PALSAR-2 achieves the full-pol mode and compact polarimetry by using the dual-pol antenna[9], which are also employed in the spaceborne P-band SAR for biomass mission of ESA[10]. However, the existing polarimetric modes mostly use the fixed dual-pol antenna, such as the horizontal/vertical linear polarization, 45°/135° linear polarization, or left-hand/right-hand circular polarization, such that it cannot adjust the transmitting/receiving polarization according to the target or the measurement environment. Therefore, they are not quite suitable for the target polarimetric characteristics measurement and research which need to address various targets in different conditions. System integration of different polarimetric modes is a way to dealing with this issue, but it will directly increase the size, the complexity, and the cost of the polarimetric radar. The method achieving dual-pol transmitting by using multi-channels switching technique cannot maximize the transmit power, namely, cannot achieve the maximum measuring distance.

A novel digital variable polarized measurement mode was proposed to address the issues mentioned above in this paper. This mode transmits arbitrary polarized electromagnetic wave by spatial polarimetric synthesis, and receives arbitrary polarized echo by digital polarimetric synthesis. Therefore, it has the ability of measuring target polarimetric characteristics under any polarized base. It is possible for the polarimetric radar to utilize any beamforming algorithm because of the digitization processing, which makes the polarimetric radar more efficient, flexible, and higher accuracy.

A W-band digital variable polarimetric radar was then designed based on the proposed mode for target polarimetric scattering characteristics research on the ground, the sea surface, and the low-altitude. Targets in those surroundings, such as the vehicles, vessels, and Unmanned Aerial Vehicles (UAVs), have the features of low RCS, small size, and low speed. Since the millimeter wave radar operates at high frequency, it has the advantages of high antenna gain, wide bandwidth, and high doppler sensibility, which makes it really suit for detecting small and slow targets in the complicated environments. The multi-channel technique was also employed in the W-band digital variable polarimetric radar. After multi-channel amplitude and phase calibration, the synthetic co-pol/cross-pol radiation pattern under linear and circular polarization were measured. Then, target experiments were conducted under the full-pol mode and the compact polarimetric mode to validate that the W-band digital variable polarimetric radar can measure the target in any polarized base and work under any existed polarization modes. Two measurement applications carried out with the radar are also presented in the paper, which are the full-pol RCS measurement of a vehicle model and the polarimetric entropy decomposition experiment in ground surroundings.

1 Theory of digital variable polarimetric radar

The main components of the digital variable polarimetric radar are the variable polarized antenna, the multi-channel T/R modules, and the digital signal processing unit, as shown in Fig. 1. The transmitting signals were spatially synthesized through the variable polarized antenna after amplitude-phase weighting on baseband in the digital signal processing unit. The receiving signals were also processed in the digital signal processing unit after DAC by the digital polarimetric synthesis.

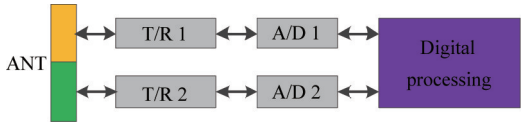

Fig. 1 Schematic diagram of digital variable polarimetric radar
图 1 数字变极化测量雷达原理框图

The basic issue of the digital variable polarimetric radar is transmitting and receiving synthesis under arbitrary polarized base. The variable polarized antenna, which is the key to deal with the issue, is an antenna array composed by two orthogonal linearly polarized subarrays, of which one is 45° linear polarization and the other is 135° linear polarization, as shown in Fig. 2. The measurement under any polarized base can be achieved by adjusting the amplitude-phase of the signals transmitted and received from the two subarrays. Let the amplitude and phase weights of each subarray be and , the weights of linear polarization and circular polarization are shown in Table 1.

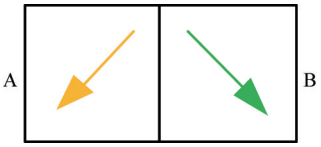

Fig. 2 Schematic diagram of variable polarimetric antenna array
图 2 变极化天线阵原理框图

Table 1 Transmitting/Receiving polarization and its amplitude-phase weights
表 1 发射/接收极化幅相加权系数表

Polarization	A_1	A_2	θ_1	θ_2
HLP	1	1	0	π
VLP	1	1	0	0
LHCP	1	1	0	π/2
RLCP	1	1	0	3π/2

The signal synthesis under any polarized base can be written as

$$\boldsymbol{E}_s = A_1\exp(j\theta_1)c_1\boldsymbol{E}_1 + A_2\exp(j\theta_2)c_2\boldsymbol{E}_2 \quad , \quad (1)$$

where $\boldsymbol{E}_1$ and $\boldsymbol{E}_2$ are the transmitting or receiving signals from the two subarrays, respectively, c_1 and c_2 are cali-

bration factors of the two channels.

In the following, the inaccuracy of polarimetric scattering matrix (PSM) measurement is considered in the digital variable polarimetric radar. Ignoring the noise, the inaccuracy of polarimetric scattering matrix measurement in the dual-channel orthogonal polarimetric radar can be described as [11]

$$\boldsymbol{Z} = \boldsymbol{RST} = \begin{bmatrix} 1 & \delta_1 \\ \delta_2 & F_1 \end{bmatrix} \begin{bmatrix} S_{HH} & S_{HB} \\ S_{VH} & S_{VV} \end{bmatrix} \begin{bmatrix} 1 & \delta_4 \\ \delta_3 & F_2 \end{bmatrix} , \quad (2)$$

where F_1 is the amplitude-phase imbalance between horizontal and vertical polarization receiving channel, and F_2 is the amplitude-phase imbalance between horizontal and vertical polarization transmitting channel. δ_1 is the cross talk of the horizontally polarized receiving antenna. δ_2 is the cross talk of the vertically polarized receiving antenna. δ_3 is the cross talk of the horizontally polarized transmitting antenna. δ_4 is the cross talk of the vertically polarized transmitting antenna. When the transmitting and receiving use the same antenna with low cross talk, we can assume that $\delta_1 = \delta_3 \approx 0$ and $\delta_2 = \delta_4 \approx 0$. Therefore, the main error of the polarimetric scattering matrix in the dual-channel orthogonal polarimetric radar is caused by the channel imbalance.

For the digital variable polarimetric radar, the transmitting and receiving wave of the horizontal polarization and vertical polarization are synthesized through the two subarrays. Therefore, the polarimetric channel imbalance does not exist, that is, $F_1 = F_2 = 1$. However, the amplitude-phase imbalance of the two T/R channels will induce high cross talk in synthesized transmitting and receiving wave, namely, δ_1, δ_2, δ_3, and δ_4 cannot be ignored. The directions of instant polarized vectors of each subarray for synthesizing the horizontal or vertical polarization are shown in Fig. 3.

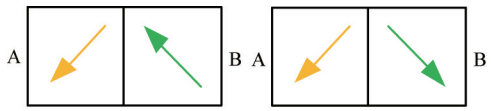

(a) 合成水平极化　　(b) 合成垂直极化

Fig. 3　Directions of instant polarized vectors in each subarray

图 3　各个子阵极化矢量瞬时方向

The channel amplitude-phase imbalances can be normalized by the amplitude-phase characteristic of channel A. Namely, the amplitude-phase characteristic of the transmitting channels can be represented by 1 and T_B, and the amplitude-phase characteristic of the receiving channels can be represented by 1 and R_B. The uniform amplitude-phase signals feed into the two T/R channels, synthesizing the horizontal polarized wave. The horizontal polarized signal is received by the two T/R channels. The synthesized horizontal polarized transmitting and receiving electromagnetic wave through the variable polarized antenna can be respectively represented by the JONES vectors as:

$$E_t^H = \frac{\sqrt{2}}{2}\begin{bmatrix} 1 + T_B \\ 1 - T_B \end{bmatrix} , \quad (3)$$

$$E_r^H = \frac{\sqrt{2}}{2}\begin{bmatrix} 1 + R_B \\ 1 - R_B \end{bmatrix} . \quad (4)$$

For synthesizing the vertical polarization, the JONES vectors also can be written respectively as

$$E_t^V = \frac{\sqrt{2}}{2}\begin{bmatrix} 1 - T_B \\ 1 + T_B \end{bmatrix} , \quad (5)$$

$$E_r^V = \frac{\sqrt{2}}{2}\begin{bmatrix} 1 - R_B \\ 1 + R_B \end{bmatrix} . \quad (6)$$

Then, the cross talk of the horizontally and vertically polarized antenna can be respectively written as

$$\begin{cases} \delta_1 = \dfrac{1 - R_B}{1 + R_B} \\ \delta_2 = \dfrac{1 - R_B}{1 + R_B} \\ \delta_3 = \dfrac{1 - T_B}{1 + T_B} \\ \delta_4 = \dfrac{1 - T_B}{1 + T_B} \end{cases} . \quad (7)$$

Hence, the inaccuracy of the polarimetric scattering matrix measurement in the digital variable polarimetric radar is described as

$$Z = \begin{pmatrix} 1 & \dfrac{1 - R_B}{1 + R_B} \\ \dfrac{1 - R_B}{1 + R_B} & 1 \end{pmatrix} \begin{pmatrix} S_{HH} & S_{HV} \\ S_{VH} & S_{VV} \end{pmatrix} \begin{pmatrix} 1 & \dfrac{1 - T_B}{1 + T_B} \\ \dfrac{1 - T_B}{1 + T_B} & 1 \end{pmatrix} . \quad (8)$$

The measurement error matrix is given as

$$\boldsymbol{S}_e = \boldsymbol{Z} - \boldsymbol{S} = \begin{pmatrix} \Delta S_{HH} & \Delta S_{HV} \\ \Delta S_{VH} & \Delta S_{VV} \end{pmatrix} . \quad (9)$$

And the error of the PSM is defined as

$$e_s = \sqrt{|\Delta S_{HH}|^2 + |\Delta S_{HV}|^2 + |\Delta S_{VH}|^2 + |\Delta S_{VV}|^2} . \quad (11)$$

The error of the PSM induced by channel amplitude-phase imbalance is shown in Fig. 4.

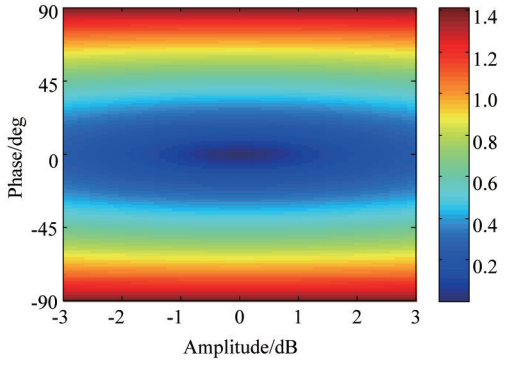

Fig. 4　Error of the measured PSM

图 4　极化散射矩阵测误差分析

2　W-band digital variable polarimetric radar

A W-band digital variable polarimetric radar was designed for target polarimetric scattering characteristics

research in the ground, the sea surface, and the low-altitude. The radar is composed of the two-subarrays variable polarized antenna, the W-band front-end with two T/R channels, two IF T/R channels and the digital signal processing unit. The variable polarized antenna is a Cassegrain antenna fed by two horn antennas. The entire radar is shown in Fig. 5.

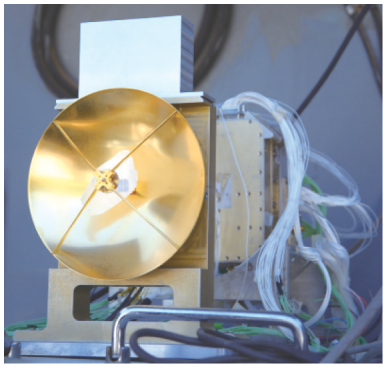

Fig. 5 W-band digital variable polarimetric radar
图 5 W 波段数字变极化测量雷达

The diagram of the channel amplitude-phase imbalance measurement is shown in Fig. 6. By using the W-band power divider and the W-band frequency converter, the amplitude-phase imbalance of the two channels was measured. Normalizing the results by channel A, T_B and R_B are obtained. The transmitting calibration factor c_n^t and receiving calibration factor c_n^r are given as

$$\begin{cases} c_1^t = c_1^r = 1 \\ c_2^t = 1/T_B, c_2^r = 1/R_B \end{cases} . \quad (11)$$

After the T/R channel amplitude-phase imbalance calibration, the linearly polarized and circularly polarized radiation patterns were measured, as shown in Fig. 7.

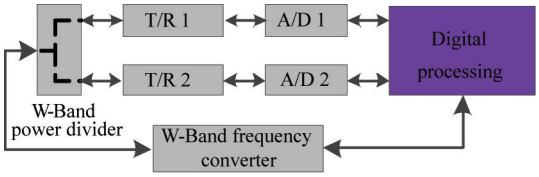

Fig. 6 Diagram of the channel amplitude-phase imbalance measurement
图 6 通道幅相不一致性测量原理框图

The cross talk of the synthesized radiation patterns after calibration is clearly better than that of the synthesized radiation patterns before calibration, as shown in Fig. 7, which demonstrates the effectiveness of the calibration. The cross talk of the linearly polarized pattern is better than that of the circularly polarized pattern, because the cross talk of the W-band standard linearly polarized horn used for radiation pattern measurement is better than that of the W-band standard circularly polarized horn. The radiation pattern measurement results illustrate that the polarized base of the radar can be changed by adjusting the amplitude-phase of the transmitting and receiving signals. Therefore, the polarization agility can be easily achieved by the rapid amplitude-phase controlling. The switching time of the polarization agility is related to the response time of the amplitude-phase controlling. Since the radar employs digitized processing, there is no time delay existing in the digital amplitude-phase controlling, so as in the polarization agility.

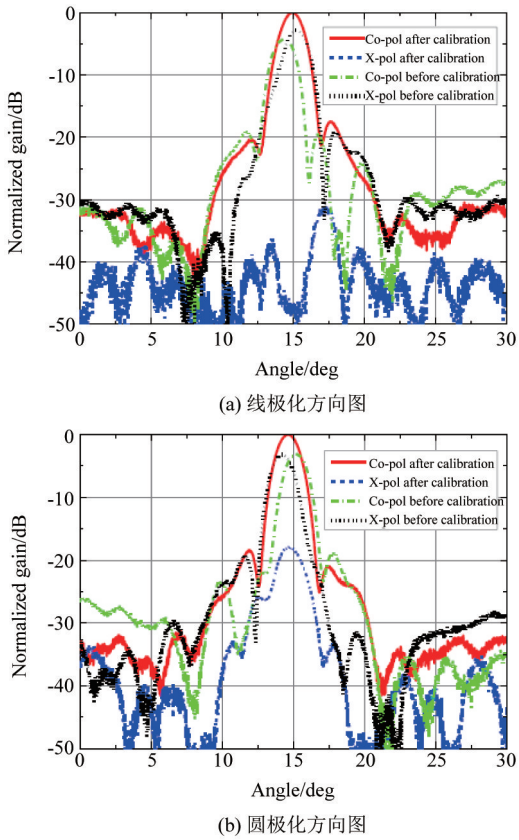

(a) 线极化方向图

(b) 圆极化方向图

Fig. 7 Radiation patterns before/after calibration
图 7 校准前后方向图测试结果

3 Target polarimetric characteristic measurement experiments

The simple point target (trihedral/dihedral corner reflectors) experiments and complex target (truck) experiment are conducted to verify the polarimetric measurement ability of the W-band digital variable polarimetric radar, as shown in Fig. 8. Two common polarized bases of polarimetric radar have been used in this experiment, which are horizontal/vertical linear polarization and left-hand/right-hand circular polarization, respectively. Full-pol and compact polarimetric modes are also achieved in the radar.

The measured values of PSM of the trihedral and dihedral corner reflectors under the full-pol mode are shown in Table 2. The compact polarimetric mode in the experiment transmits left-hand circular polarized wave and receives the horizontal/ vertical linear polarization of the echo. The measured values are shown in Table 3. The results are very close to the theoretical value. The full-pol HRRPs of the truck under linearly/circularly polarized base are shown in Fig. 9. The HRRPs under linearly polarized base are clearly different from those under

(a) 三面角反射器　　(b) 二面角反射器

(c) 卡车

Fig. 8　Experiment targets
图 8　实验目标

circularly polarized base. Several scattering centers can be found along the high-resolution range in the HRRPs, which have various polarimetric scattering features. The first scattering center shows a classical single-bounce scattering feature which is induced by the plane of the truck head. The results illustrate that the W-band digital variable polarimetric radar has the ability of measuring target under any polarized base, and easily achieves the full-pol mode and compact polarimetric mode.

Table 2　The results of PSM measurement in full-pol mode
表 2　全极化体制下极化散射矩阵测量结果

	Theoretical values	Measurement values	Errors
TCR (H-V base)	(1, 0, 0, 1)	(1, 0.02 + 0.00j, 0.03 + 0.02j, 0.93 + 0.07j)	0.1072
TCR (L-R base)	(0, 1, 1, 0)	(-0.04 - 0.02j, 0.91 + 0.06j, 1, -0.03 - 0.01j)	0.1212
DCR (H-V base)	(1, 0, 0, -1)	(1, -0.17 + 0.15j, 0.10 - 0.10j, -1.17 - 0.42j)	0.5260
DCR (L-R base)	(1, 0, 0, -1)	(1, 0.13-0.13j, 0.03 + 0.06j, -1.04 -0.32j)	0.3772

Table 3　The results of PSM measurement in compact polarimetric mode
表 3　紧凑极化体制下极化散射矩阵测量结果

	Theoretical values	Measurement values	Errors
TCR	(1, -j)	(1, -0.14 - 0.90j)	0.172 0
DCR	(1, j)	(1, -0.15 + 0.89j)	0.186 0

A RCS measurement of a vehicle model is also conducted under the full-pol mode using the linearly polarized base. The RCS values with a bandwidth of 800 MHz were measured. The full-pol normalized RCS values versus different azimuth angles are shown in Fig. 10. It can be seen that the RCS values of the head, side, and trail of the vehicle model are more higher than that of the rest

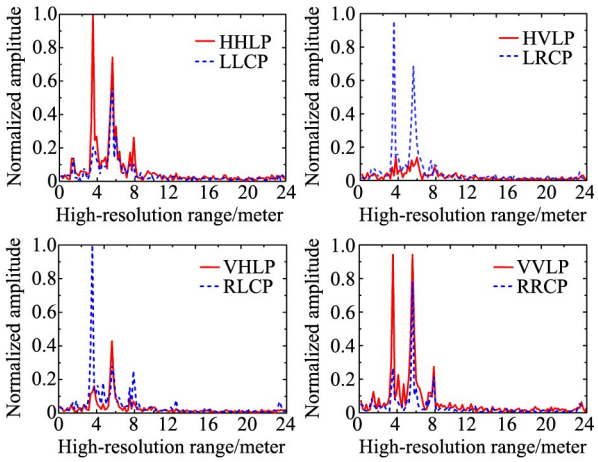

Fig. 9　Full-pol HRRPs of a truck under linearly/circularly polarized base
图 9　线/圆极化基下卡车全极化一维高分辨距离像

parts. In addition, the RCS values in cross-pol channels are about 15 dB lower than that in co-pol channels. A simple polarimetric processing was applied in this experiment, which is taking addition and subtraction between the HH-channel and VV-channel. The addition of HH and VV will increase the amplitude of the single bounce scattering, while the subtraction of HH and VV will increase the amplitude of the double bounce scattering, as shown in Fig. 11.

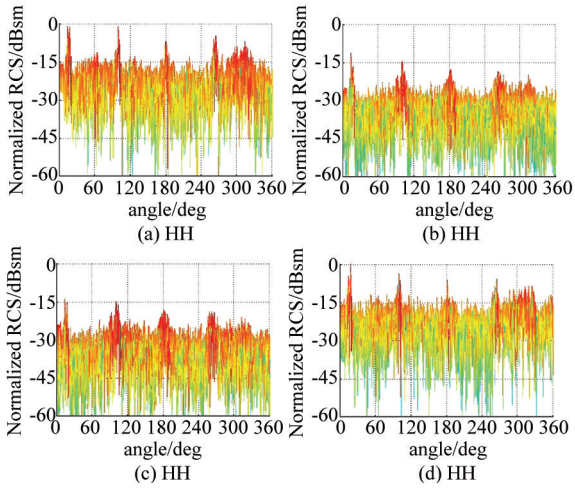

Fig. 10　Normalized RCS of the vehicle model under linearly polarized base. (the noise floor is lower than -40 dBsm)
图 10　线极化基下小车模型归一化 RCS 测量结果(底噪低于-40 dBsm)

The polarimetric entropy decomposition is a classical polarimetric target decomposition theory, which describes the randomness and the mechanism of scattering of the radar target. Combining the high-resolution technique, we utilized the difference of the scattering randomness between the natural and the man-made target to detect the man-made target in heavy ground clutter. The targets in the experiment scene are as follows: a truck, a trihedral corner reflector located at 5 meters ahead of the

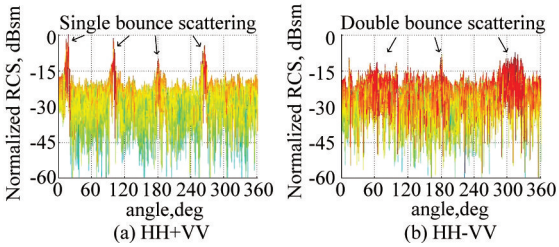

Fig. 11 Polarimetric processing. (the noise floor is lower than -40 dBsm)
图 11 极化处理(底噪低于-40 dBsm)

truck, the walls and bush located at about 100 meters behind the truck. The full-pol HRRPs are shown in Fig. 12. The amplitude of echo of the walls is higher than that of the truck, which is unfavorable for the detection of the truck. By applying the polarimetric entropy decomposition in the full-pol HRRPs, the entropy H and mean scattering angle α in high-resolution range are shown in Fig. 13. Three conclusions can be drawn as follows:

1) The truck, trihedral corner reflector and walls have low entropy, while the bush has relatively high entropy. This is determined by the target scattering randomness.

2) The entropy values of truck are low in continuous range cells, while the trihedral corner reflector and walls present as a point scattering.

3) The mean scattering angle in each range cells of the truck varies greatly compared with that of the trihedral corner reflector and walls. This is because the truck has multiple scattering mechanisms while the trihedral corner reflector and walls mainly present as a single-bounce scattering.

After extracting the length of each low-entropy region, calculating the mean values of entropy and scattering angle of each low-entropy region, the location of the truck can be extracted correctly from the full-pol HRRPs by combining these parameters, as shown in Fig. 14.

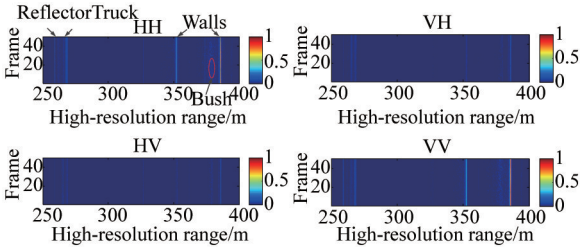

Fig. 12 Full-pol HRRPs of the experimental scene
图 12 实验场景的全极化一维高分辨距离像

4 Conclusions

A W-band digital variable polarimetric radar for target polarimtric characteristic research is presented in this paper. This radar transmits arbitrary polarized electromagnetic wave by spatial polarimetic synthesis, and receives arbitrary polarized echo by digital polarimetic synthesis. The measurements of radiation patterns, PSMs of corner reflectors and full-pol HRRPs of a truck along

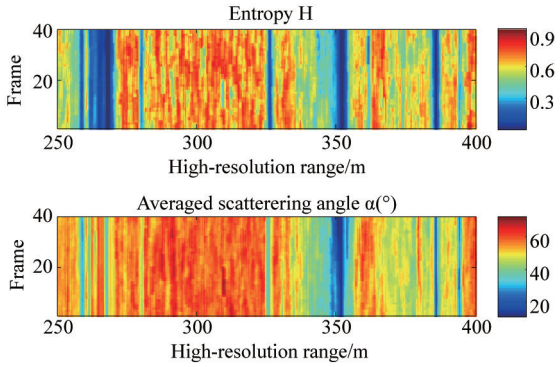

Fig. 13 Polarimetric entropy decomposition
图 13 极化散射熵分解

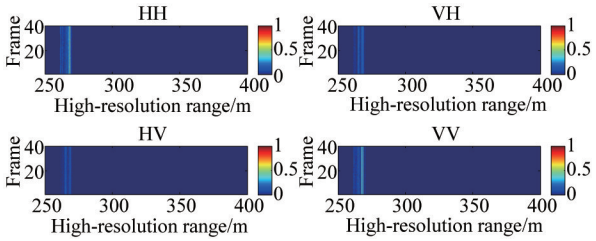

Fig. 14 Full-pol HRRPs after detection by combining polarimetric parameters
图 14 检测后的全极化高分辨一维距离像

with the RCS measurement of a vehicle model and the target polarimetric entropy decomposition experiment illustrate that the W-band digital variable polarimetric radar has the ability of measuring target polarimetric characteristic under any polarized base, and can easily achieves any existing polarization mode. The radar can satisfy the various needs of the polarmetric measurement applications, which is suitable for the target polarimetric characteristic measurement and research.

References

[1] Cloude S R., Pottier E. An entropy based classification scheme for land applications of polarimetric SAR [J]. IEEE Transactions on Geoscience and Remote Sensing, 1997, **35**(1), 68-78.

[2] Yanovsky F J, Russchenberg H W J, Unal C. M. H. Retrieval of information about turbulence in rain by using Doppler-polarimetric Radar [J]. IEEE Transactions on Microwave Theory and Techniques, 2005, **53**(2), 444-450.

[3] Park J, Johnson J Majurec, N, *et al*. Simulation and analysis of polarimetric radar signatures of human gaits [J]. IEEE Transactions on Aerospace and Electronic Systems, 2014, **50**(3), 2164-2175.

[4] Schimpf H. Essen, H, Boehmsdorff S, *et al*. MEMPHIS-a fully polarimetric experimental radar: IEEE International Geoscience and Remote Sensing Symposium, 2002 [C]. Toronto, 2002: 3, 1714-1716.

[5] Danklmayer A, Biegel G, Brehm T, *et al*. Millimeter wave propagation above the sea surface during the Squirrel campaign: International Radar Symposium, 2015[C]. Dresden, 2015: 300-304.

[6] Martin-Neira M. Ribo, S. Martin-Polegre. A. J. Polarimetric mode of MIRAS [J]. IEEE Transactions on Geoscience and Remote Sensing, 2002, **40**(8), 1755-1768.

(下转第 113 页)

本文算法对数据在沿飞行方向的二维剖面单独进行滤波处理,考虑到光子计数激光雷达在垂轨方向有多个探测器.下一步将考虑结合相邻探测器的数据进行三维滤波,同时结合地面与植被冠层的高程差信息以进一步提高稀疏植被冠层的滤波精度.

5　结论

基于离散化的回波点的在地物起伏方向具有更大密度的特性,提出一种算法基于回波的密度和形态特征的自适应滤波方向的点云滤波方法.主要解决回波稀疏区域的信号与噪声分离问题,具有较高的地形适应性.

通过实验数据对算法进行了验证,所提出的滤波算法能有效剔除与地面非常接近的噪声点,且具有较高的滤波精度.实验结果表明,植被和地面回波数据的滤波综合精度达到94.87%,其中地面滤波精度达到97.89%.算法较好的满足了光子计数激光雷达数据滤波的实用需求,提高了点云产品的高程精度.

References

[1] ZHU Lei, HUANG Geng-Hua, OUYANG Jun-Hua, *et al*. STUDY ON TIME INTERVAL MEASUREMENT SYSTEM IN PHOTON COUNTING IMAGING LIDAR[J]. *J. Infrared Millim. Waves* (朱磊, 黄庚华, 欧阳俊华, 等. 光子计数成像激光雷达时间间隔测量系统研究[J]. **红外与毫米波学报**), 2008, **27**(6):461 - 464.

[2] Abshire J B, Sun X, Riris H, *et al*. Geoscience Laser Altimeter System (GLAS) on the ICESat Mission: On-orbit measurement performance[J]. *Geophysi- cal Research Letters*, 2005, **32**(21): 365 - 370.

[3] Brunt K M, Neumann T A, Walsh K M, *et al*. Determination of Local Slope on the Greenland Ice Sheet Using a Multibeam Photon-Counting Lidar in Preparation for the ICESat-2 Mission[J]. *IEEE Geoscience & Remote Sensing Letters*, 2014, **11**(5):935 - 939.

[4] Dautet H, Deschamps P, Dion B, *et al*. Photon-counting techniques with silicon avalanche photodiodes[J]. *Applied Optics*, 1993, **32**(21):3894 - 900.

[5] Matthew M G, Dennis H, William H, *et al*. Cloud Physics Lidar: Instrument Description and Initial Measurement Results[J]. *Applied Optics*, 2002, **41**(18):3725 - 34.

[6] Yuekui Yang, Alexander Marshak, Stephen P. Palm, *et al*. Cloud Impact on Surface Altimetry From a Spaceborne 532-nm Micropulse Photon-Counting Lidar: System Modeling for Cloudy and Clear Atmospheres[J]. *IEEE Transactions on Geoscience & Remote Sensing*, 2011, **49**(12): 4910 - 4919.

[7] Brif C. Reduction of optimum light power with Heisenberg-limited photon-counting noise in interferometric gravitational-wave detectors [J]. *Physics Letters A*, 1999, **263**(1): 15 - 20.

[8] XIA Shaobo, WANG Cheng, XI Xiaohuan, LUO Shezhou, et al. Point cloud filtering and tree height estimation using airborne experiment data of ICESat-2[J], *Journal of Remote Sensing*(夏少波, 王成,习晓环,等. ICESat-2 机载试验点云滤波及植被高度反演[J]. **遥感学报**),2014,**18**(6):1199 - 1207.

[9] Sui Lichun . Analysis of Laser Scanner Data by Means of Digital Image Processing Techniques[M]. Munich, Germany: Publishing House,2003.

[10] Horan K H, Kerekes J P. An automated statistical analysis approach to noise reduction for photon-counting lidar systems[C]// Geoscience and Remote Sensing Symposium (IGARSS), 2013 IEEE International. IEEE, 2013:4336 - 4339.

[11] Awadallah M, Ghannam S, Abbott L, et al. Active Contour Models for Extracting Ground and Forest Canopy Curves from Discrete Laser Altimeter Data[C]//13th International Conference on Lidar Applications for Assessing Forest Ecosystems, 2013.

[12] Albota M A, Heinrichs R M, Kocher D G, *et al*. Three-dimensional imaging laser radar with a photon-counting avalanche photodiode array and microchip laser[J]. *Applied Optics*, 2003, **41**(36): 7671 - 8.

[13] Rosette J, Field C, Nelson R, *et al*. A new photon-counting lidar system for vegetation analysis[C]// Proceedings of SilviLaser 2011, 11th International Conference on LiDAR Applications for Assessing Forest Ecosystems, University of Tasmania, Australia, 16 - 20 October 2011.

[14] Zhang J, Kerekes J P. First-Principle Simulation of Spaceborne Micropulse Photon-Counting Lidar Performance on CoMBLex Surfaces[J]. *IEEE Transactions on Geoscience & Remote Sensing*, 2014, **52**(10):6488 - 6496.

[15] Zhang J, Kerekes J, Csatho B, *et al*. A clustering approach for detection of ground in micropulse photon-counting LiDAR altimeter data[C]// Geoscience and Remote Sensing Symposium (IGARSS), 2014 IEEE International. IEEE, 2014: 177 - 180.

(上接第 40 页)

[7] Drake P. R, Bourgeois J, Hopf A. P. *et al*. Dual-polarization X-band phased array weather radar Technology update: International Radar Conference, 2014[C]. Lille, 2014: 1 - 6.

[8] Nord M. E, Nord M. E, Ainsworth T. L, *et al*. Comparison of Compact Polarimetric Synthetic Aperture Radar Modes [J]. IEEE Transactions on Geoscience and Remote Sensing, 2009, **47**(1), 174 - 188.

[9] Okada Y, Nakamura S, Iribe K, *et al*. System characteristics for wide swath L-band SAR onboard ALOS-2/PALSAR-2: Asia-Pacific Conference on Synthetic Aperture Radar, 2013 [C]. Tsukuba, 2013: 141 - 143.

[10] Ramongassie S, Castiglioni S. K. Lorenzo, J, *et al*. Spaceborne P-band SAR for BIOMASS mission: IEEE International Geoscience and Remote Sensing Symposium , 2010[C]. Honolulu, 2010, 2880 - 2883.

[11] van Zyl J. J. Calibration of polarimetric radar images using only image parameters and trihedral corner reflector responses [J]. IEEE Transactions on Geoscience and Remote Sensing, 1990, **28**(3), 337 - 348.